Structural Durability & Health Monitoring

Tech Science Press

https://doi.org/10.32604/sdhm.2026.079457

ARTICLE

Thermo-Mechanical Behavior and Residual Strength of Reinforced Concrete Beams under Fire Exposure

Hongyan Liu, Fang Wang, Jie Zhao and Feng Wu*

School of Architecture and Design, Yunnan Technology and Business University, Kunming, China

*Corresponding Author: Feng Wu. Email: wf678888@163.com

Received: 21 January 2026; Accepted: 22 April 2026; Published: 24 August 2026

ABSTRACT: This study investigates the thermo-mechanical behavior and residual strength of full-scale reinforced concrete (RC) beams subjected to ISO-834 fire exposure, emphasizing temperature-dependent material degradation and bond-slip effects. A sequentially coupled numerical framework was developed in ABAQUS, integrating a temperature-indexed Concrete Damage Plasticity (CDP) model for concrete, elastoplastic steel constitutive laws, and a temperature-dependent bond-slip model implemented via nonlinear SPRING2 elements. The model explicitly accounts for post-peak concrete softening, steel yield degradation, and interface deterioration, and was calibrated against full-scale experiments. Experimental measurements included internal and surface temperatures, load–midspan deflection, and residual strength after natural cooling. The numerical results closely reproduce the experimental observations, with deviations of 7%–10% for both mid-span deflection and ultimate load. Key findings include: C40 concrete retains ~60% of its ambient compressive strength at 300°C–400°C; stiffness and peak load decrease by 30%–70% and 40%–50% at 600°C, respectively; residual load capacity drops to 20%–25% at 700°C. Steel yield strength decreases by ~50% at 600°C, and bond deterioration accelerates deflection and reduces residual capacity. This integrated numerical–experimental framework provides a validated predictive tool for post-fire performance assessment of RC beams, supporting fire-resilient design and structural safety evaluation.

KEYWORDS: Thermo-mechanical coupling; reinforced concrete; fire resistance; concrete damage plasticity (CDP); bond-slip; residual strength

1 Introduction

The fire performance of reinforced concrete (RC) structures is a critical concern in both research and engineering practice. Concrete exhibits significant reductions in compressive strength and stiffness under elevated temperatures, while steel reinforcement suffers substantial yield strength loss. These thermo–mechanical (TM) effects can markedly reduce residual load-bearing capacity, potentially leading to premature failure during or after fire exposure. Quantitative studies indicate that C40 concrete retains approximately 60% of its ambient compressive strength at 300°C–400°C, decreases to 30%–40% at 500°C–600°C, and falls below 20%–25% beyond 700°C–800°C, whereas steel yield strength reduces by roughly 50% at 600°C. Full exposure to ISO-834 fire for two hours typically results in a 30%–40% reduction in residual load capacity, accompanied by accelerated mid-span deflections due to stiffness loss and bond deterioration.

Numerical modeling has advanced to simulate these TM behaviors. Sequentially coupled finite element models, temperature-dependent Concrete Damage Plasticity (CDP), cohesive interface models, and bond-slip formulations have been developed to predict deflection, cracking, and residual load capacity. Table 1 summarizes representative recent studies, highlighting modeling approaches, structural systems, and key contributions.

Table 1: Recent studies for TM modelling of concrete.

Authors (Year)	Focus/Model	Key contribution
Saha et al. (2025) [1]	TM analysis at spalling onset	Links H-TRIS tests with TM stresses at spalling under ISO vs. hydrocarbon fires; explores uni-/biaxial load effects.
Hesien et al. (2025) [2]	Full-scale flat plate; CDP calibration	Compares shell vs. solid strategies; shows sensitivity to dilation and tensile law; examines top/bottom fire exposure.
Li et al. (2024) [3]	CFST stub columns, sequential coupling	Validates a TM workflow and quantifies residual axial resistance vs. fire time/load level/confinement.
Zhang et al. (2022) [4]	Cohesive interface + heat conduction	Simulates thermal-induced explosive spalling at meso-scale with cohesive elements.
Feng et al. (2026) [5]	Thermodynamically consistent damage-plasticity model	Unified thermo-mechanical framework enabling fire-resistant design and optimization.
Tang et al. (2025) [6]	ST-RC columns after one-side fire	Post-fire cyclic response modelling; quantifies stiffness/ductility degradation.
Feng et al. (2025) [7]	Temperature-indexed concrete damage plasticity framework for thermo–mechanical analysis	Simplified temperature-dependent constitutive model enabling efficient thermo–mechanical analysis of concrete structures.
Ning et al. (2025) [8]	CDP for lattice-reinforced cement composites	Temperature-dependent composite behavior; shows limited polymer-lattice contribution near peak stress.
Lu et al. (2021) [9]	Coupled thermo-mechanical damage modelling for steel structures in fire	Proposed a validated thermo-mechanical damage model for fire-affected steel structures.
Gernay et al. (2023) [10]	CDP + Thermo-mechanical (Fire + static load)	Incorporated cooling phase effects.

Despite these contributions, most studies do not include full-scale beam validation, temperature-indexed bond-slip degradation, or post-fire residual performance, motivating the present work.

In this study, the thermo–mechanical response of full-scale RC beams under ISO-834 fire is investigated using a validated numerical–experimental framework. A sequentially coupled FEM model in ABAQUS incorporates temperature-indexed CDP parameters for concrete, elastoplastic steel constitutive laws, and an explicit temperature-dependent bond-slip mechanism. Full-scale experiments include internal and surface temperature monitoring and residual strength evaluation after natural cooling. Comparisons between numerical predictions and experimental measurements show strong agreement (7%–10% deviation in mid-span deflection and load–deformation behavior), capturing concrete strength reduction (≈25%–40% at 500°C–600°C, >70% beyond 800°C) and steel yield strength loss (~50% at 600°C), resulting in approximately 30%–40% reduction in residual load capacity. This integrated approach provides a practical tool for post-fire performance assessment and fire-resilient design of RC members, highlighting the impact of stiffness degradation and bond deterioration on structural safety.

2 Materials and Methods

2.1 Specimen Parameters

Three full-scale reinforced concrete (RC) beam specimens (L1, L2, and L3) were tested under three-sided ISO-834 fire exposure [11]. Each beam had a total length of 4000 mm with a clear span of 3600 mm and a cross-section of 250 mm × 400 mm. Longitudinal reinforcement consisted of four 25 mm diameter HRB400 bars at the bottom (yield strength ≈ 451 MPa) and two 16 mm diameter HRB400 bars at the top (yield strength ≈ 445 MPa). Shear reinforcement consisted of 8 mm diameter stirrups (yield strength ≈ 380 MPa) spaced at 150 mm in high-moment regions. Concrete had an ambient compressive strength of 40.2 MPa, measured from standard cylinders at 28 days, while the design compressive strength used for structural calculations was 17.1 MPa. The elastic modulus at ambient temperature was 31.5 GPa. The longitudinal and shear reinforcement ratios were 1.96% and 0.27%, respectively.

The bottom and two side faces of the beams were exposed to the fire, while the top face and a 100 mm zone near each support were thermally insulated to simulate realistic boundary conditions. Fire exposure followed the ISO-834 standard fire curve for 2 h, as specified in GB 51249–2017. Experimental measurements, including deflection, temperature distribution, and residual strength after natural cooling, were used to validate the numerical model (Fig. 1).

2.2 Cooling Curve

The post-fire cooling process consisted of two stages (Fig. 2), a holding stage of 3 h at the peak temperature (heating rate 5°C/min), followed by natural cooling over 24 h to ambient temperature. Residual strength was evaluated at the end of cooling to capture post-fire performance.

2.3 Stress-Strain Curves of Concrete

Stress–strain curves of concrete at 20°C, 200°C, 400°C, 600°C, and 800°C were obtained experimentally (Fig. 3). The curves illustrate the reduction in peak compressive stress and increase in post-peak strain with increasing temperature, highlighting thermal softening and enhanced ductility critical for fire-exposed RC beams.

2.4 Numerical Modeling Approach

A sequentially coupled thermal–structural analysis approach was used to explore the behavior of RC beams under elevated temperatures. The numerical model was developed in two stages: (1) a heat transfer (temperature field) analysis to determine the temperature distribution in the beam over time, followed by (2) a structural (force field) analysis using the temperature-dependent material properties to simulate the mechanical response of the beam.

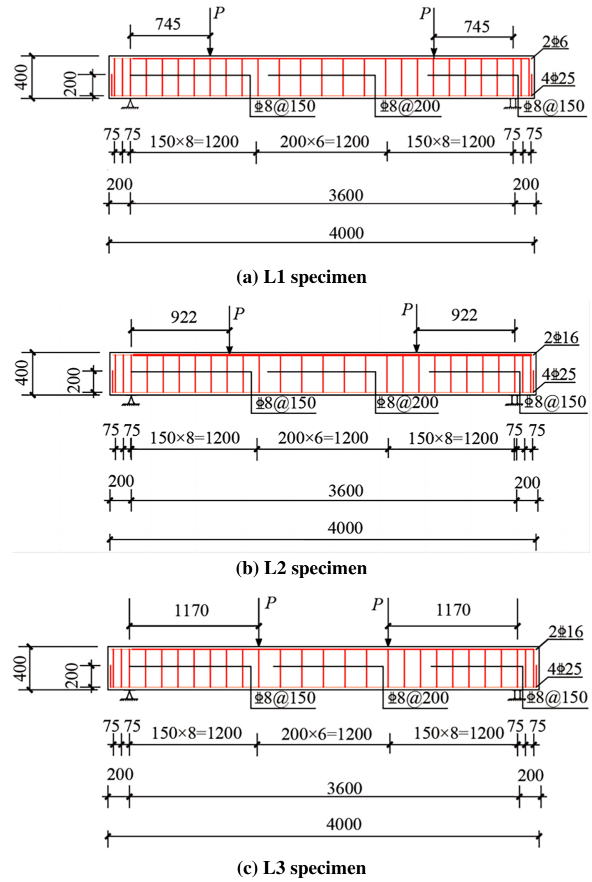

Figure 1: Geometry and reinforcement details of full-scale RC beam specimens (L1–L3).

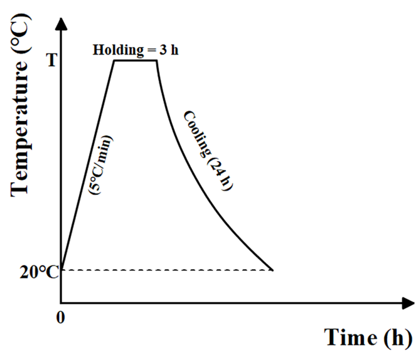

Figure 2: Temperature-time cooling curve of RC beams after fire exposure.

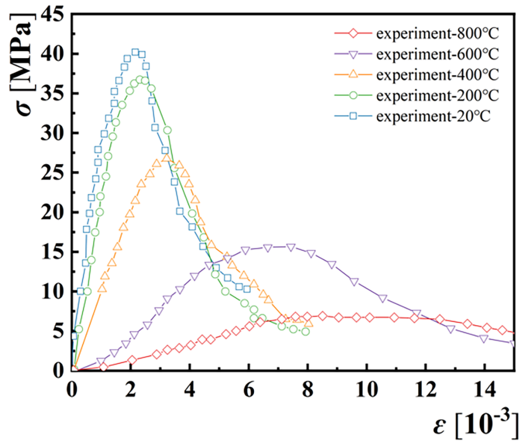

Figure 3: Stress–strain curves of concrete at different temperatures.

A transient heat transfer simulation was performed on the 3D beam model to capture the temperature variation across the beam cross-section and along its length during fire exposure. The concrete was modeled with 8-node linear heat transfer solid elements (DC3D8 in ABAQUS), and the steel reinforcement was modeled with 2-node linear heat transfer rod elements (DC1D2) embedded in the concrete mesh. Tie constraints were applied between concrete and steel heat transfer meshes so that both materials shared temperature fields. The initial uniform temperature of the entire model was 20°C. The fire was applied on the bottom and two vertical faces of the beam as time-dependent boundary conditions of convective and radiant heat flux. For the exposed surfaces, a convection coefficient of 25 W/(m^2·K) (equivalent to 2100 J/(m^2·min·°C)) was used along with an ambient gas temperature following the ISO 834 fire curve. An emissivity of 0.5 was assumed for thermal radiation exchange on exposed surfaces. The top face and the end regions (within 100 mm of supports) were treated as thermally insulated (unexposed), with a lower convection coefficient of 9 W/(m^2·K) (≈600 J/(m^2·min·°C)) and no direct heating. The standard ISO 834 fire temperature as a function of time t (in minutes) is given by the empirical formula from the code [12]:

$$T_{ISO0834} = 345lg\left(8t + 1\right) + T_0 \tag{1}$$

The mechanical analysis was initiated after computing the transient temperature field. The temperature results (node temperatures) at selected time points were imported into a structural model of the same beam (sequential coupling). In the structural model, concrete was modeled with 8-node 3D solid elements with reduced integration (C3D8R in ABAQUS), and steel reinforcement with 2-node truss elements (T3D2). To accurately capture the bond–slip effect between steel and concrete at high temperature, the default perfect bond assumption was modified. The embedded constraint tying the steel nodes to concrete was released for the longitudinal bars, and nonlinear spring elements were introduced at the steel–concrete interface to simulate the bond behavior [13]. These springs, acting in the axial direction of the bars (and in two transverse directions for dowel action), were calibrated to represent the temperature-dependent bond stress–slip relationship [14]. The bond between stirrups and concrete was assumed to remain intact (stirrups primarily provide shear confinement). The mechanical loading on the beam was applied incrementally under transient high-temperature conditions: a sustained service load (vertical mid-span load) was applied at the beginning of the structural analysis and kept constant while the material properties were degraded according to the rising temperatures [15]. Supports were modeled as simple supports allowing rotation. Geometric nonlinearity was included to capture any large deflection effects.

The mesh and element topology for the structural model matched that of the thermal model to ensure consistent node mapping for temperature data. Mesh sizes 5–10 mm; convergence study confirmed results were mesh-independent (<5% deviation in deflection and stress) [16]. Fig. 4 illustrates the finite element model configuration, including the mesh and boundary conditions, as used for the mechanical analysis under elevated temperatures.

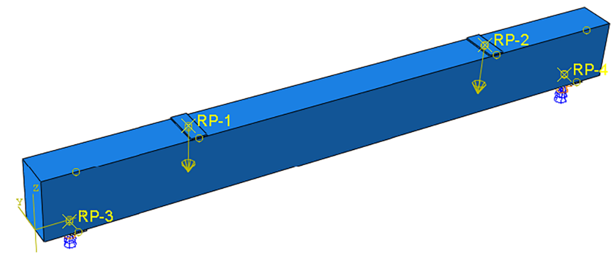

(a) Concrete model and boundary conditions

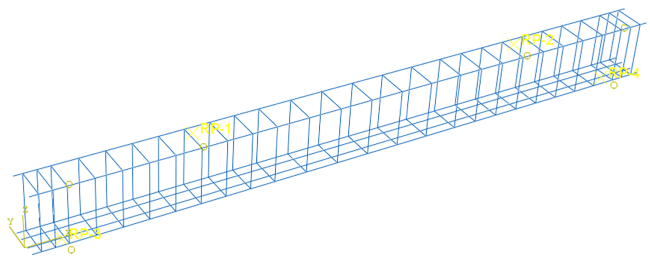

(b) Rebar model

Figure 4: Finite element model for thermal–mechanical analysis (ABAQUS).

It is noteworthy that similar numerical modeling approaches have been successfully applied to fire performance studies of other structural systems—for instance, to restrained composite beams under fire—demonstrating the broad applicability of sequentially coupled thermal–structural simulations in fire engineering analysis.

2.5 Constitutive Model of Concrete under Fire Exposure

Concrete exposed to elevated temperatures undergoes significant degradation in its mechanical properties. High temperatures reduce the compressive and tensile strength as well as the elastic modulus, while simultaneously increasing deformability. For example, normal-weight concrete may retain only 30%–40% of its ambient compressive strength at approximately 600°C, and the elastic modulus exhibits similar or greater relative reductions, resulting in a flatter initial slope in the stress–strain curve [17]. These changes arise from thermal cracking, moisture evaporation, and other microstructural damage mechanisms that develop under fire conditions.

To capture this behavior in numerical simulations, a temperature-indexed concrete constitutive model was developed based on Eurocode 2 (EN 1992-1-2) formulations. Unlike standard design-oriented Eurocode models, this approach explicitly parameterizes compressive strength, tensile strength, and elastic modulus as continuous functions of temperature and incorporates post-peak strain evolution to reflect enhanced ductility at high temperatures [18]. This customized constitutive law is implemented in ABAQUS CDP, enabling realistic simulation of stiffness degradation, thermal softening, and post-peak behavior under ISO-834 fire exposure. The temperature-dependent CDP model parameters adopted in the numerical simulation are summarized in Table 2.

Table 2: Temperature-dependent CDP model parameters.

Temperature (°C)	Dilation angle ψ (°)	Flow eccentricity ε	fb0/fc0 ratio	Viscosity parameter μ
20	36	0.10	1.16	0.001
200	34	0.10	1.16	0.001
400	32	0.10	1.16	0.001
600	28	0.10	1.16	0.001
800	24	0.10	1.16	0.001

Compressive strength degradation:

$$f_{c,\theta}(T) = k_c(T) f_c(20°\mathrm{C}) \tag{2}$$

where $f_c(20°\mathrm{C})$is the ambient compressive strength, and $k_c(T)$ is the reduction factor:

$$k_c(T) = \begin{cases} 1, 20 \le T < 100°\mathrm{C} \\ 1 - 0.002(T - 100), 100 \le T < 200°\mathrm{C} \\ 0.8 - 0.001(T - 200), 200 \le T < 400°\mathrm{C} \\ 0.6 - 0.001(T - 400), 400 \le T < 600°\mathrm{C} \\ 0.4 - 0.001(T - 600), 600 \le T < 800°\mathrm{C} \\ 0.2\ T \ge 800°\mathrm{C} \end{cases} \tag{3}$$

Peak and ultimate strains:

$$\varepsilon_{c1,\theta}(T) = \varepsilon_{c1}(20°\mathrm{C})\left[1 + 0.002 \cdot \left(\frac{T}{100}\right)\right] \tag{4}$$

$$\varepsilon_{cu,\theta}(T) = \varepsilon_{cu}(20°\mathrm{C})\left[1 + 0.01 \cdot \left(\frac{T}{100}\right)\right] \tag{5}$$

Stress–strain law:

$$\frac{\sigma_c}{f_{c,\theta}} = \begin{cases} \dfrac{\varepsilon}{\varepsilon_{c1,\theta}} - \left(\dfrac{\varepsilon}{\varepsilon_{c1,\theta}}\right)^2, 0 \le \varepsilon \le \varepsilon_{c1,\theta} \\ \dfrac{\varepsilon_{cu,\theta} - \varepsilon}{\varepsilon_{cu,\theta} - \varepsilon_{c1,\theta}}, \varepsilon_{c1,\theta} \le \varepsilon \le \varepsilon_{cu,\theta} \\ 0, \varepsilon > \varepsilon_{cu,\theta} \end{cases} \tag{6}$$

This formulation ensures that the ABAQUS CDP model captures concrete stiffness degradation, peak strength reduction, and increased post-peak deformability relevant for fire-exposed RC beams. Tensile strength above ~300°C is considered negligible due to extensive cracking, consistent with experimental observations.

2.6 Constitutive Model of Reinforcement Steel under Fire Exposure

Reinforcing steel also exhibits significant temperature-dependent degradation. While remaining ductile, its yield strength and elastic modulus decrease sharply above 400°C–500°C [19]. At ~600°C, steel retains only 30%–40% of its ambient yield strength, and the modulus reduces to a similar fraction. To accurately capture this behavior in numerical simulations, the steel constitutive law was developed from Eurocode 2 empirical formulations, parameterized as temperature-dependent functions suitable for sequential thermo-mechanical FEM analysis [20].

Yield strength degradation:

$$f_{y,\theta}(T) = k_y(T)\, f_y(20^\circ\mathrm{C}) \tag{7}$$

$$k_y(T) = \begin{cases} 1, 20 \le T < 400^\circ\mathrm{C} \\ 1 - 0.0033(T - 400), 400 \le T < 600^\circ\mathrm{C} \\ 0.33 - 0.00165(T - 600), 600 \le T < 800^\circ\mathrm{C} \\ 0, T \ge 800^\circ\mathrm{C} \end{cases} \tag{8}$$

Elastic modulus reduction:

$$E_{s,\theta}(T) = k_E(T)\, E_s(200^\circ\mathrm{C})$$

$$k_E(T) = \begin{cases} 1, 20 \le T < 100^\circ\mathrm{C} \\ 1 - 0.001(T - 100), 100 \le T < 600^\circ\mathrm{C} \\ 0.5 - 0.0005(T - 600), 600 \le T < 800^\circ\mathrm{C} \\ 0.2, T \ge 800^\circ\mathrm{C} \end{cases} \tag{9}$$

Stress–strain law:

$$\sigma_s(\varepsilon, T) = \begin{cases} E_{s,\theta}(T)\,\varepsilon, 0 \le \varepsilon \le \varepsilon_{y,\theta}(T) \\ f_{y,\theta}(T), \varepsilon_{y,\theta}(T) < \varepsilon \le \varepsilon_{su,\theta}(T) \\ 0, \varepsilon > \varepsilon_{su,\theta}(T) \end{cases} \tag{10}$$

This customized temperature-indexed steel model ensures that the FEM simulation captures the progressive loss of tensile capacity and stiffness under fire, providing a reliable basis for the sequential thermo-mechanical analysis of RC beams.

2.7 ABAQUS Spring Elements for Simulating Bond Behavior and Temperature Effects

To capture the interface behavior between reinforcement steel and concrete under fire exposure, a temperature-indexed bond-slip model was developed and implemented in ABAQUS using SPRING2 elements [21]. These spring elements are positioned at the interface nodes between the concrete solid elements and the reinforcement beam elements, transmitting shear stresses as relative slip occurs along the steel–concrete interface. This approach allows the model to explicitly account for progressive bond degradation and the impact of elevated temperatures on the load transfer between steel and concrete.

The stiffness of each spring element is directly linked to the bond strength, and it is adjusted according to temperature using a continuous degradation function:

$$K(T) = k_0 D(T) \tag{11}$$

where k_0 is the initial stiffness of the spring, and $D(T)$ is the temperature-dependent degradation factor, which is defined as:

$$D(T) = 1 - 0.5\left(\frac{T}{T_{max}}\right) \tag{12}$$

Tmax represents the maximum temperature. As the temperature increases, the bond stiffness gradually decreases, eventually leading to complete failure at elevated temperatures.

The bond strength $\tau(T)$ is similarly scaled with temperature using the same degradation factor $D(T)$, allowing the spring elements to realistically simulate the reduction in shear transfer capacity along the interface. At ambient conditions (20°C), the bond strength is maximal, while at high temperatures, the bond strength gradually declines, capturing the progressive loss of composite action between steel and concrete [22]. This customized temperature-indexed bond-slip formulation enables ABAQUS to replicate the observed bond-slip behavior under fire, providing a robust framework for sequential thermo-mechanical simulation of RC beams.

3 Results

3.1 Shear and Flexural Capacity under Thermo-Mechanical Coupling

To assess the structural performance of RC beams under combined fire exposure and mechanical loading, both shear and flexural capacities were analyzed. While shear capacity provides a preliminary check, the primary focus is on mid-span flexural behavior, as this governs failure under four-point bending.

Temperature-dependent concrete compressive strength $f_c(T)$ and steel yield strength $f_y(T)$ were used to calculate sectional capacities. At mid-span, equilibrium of internal forces and moments, accounting for thermal degradation of material properties, yields a first-order estimation of shear and flexural capacities.

According to the force balance formula, as shown in Fig. 5:

$$\sum X = 0, \sigma_c(T)\, b\xi h_0 = A_s\sigma_s(T) \tag{13}$$

$$\sum Y = 0, \tau_c(T)\, b\xi h_0 = AV_c(T) \tag{14}$$

$$\sum M = 0, \sigma_c(T)\, b\xi h_0 (h_0 - 0.5\xi h_0) = V_c(T)\, a \tag{15}$$

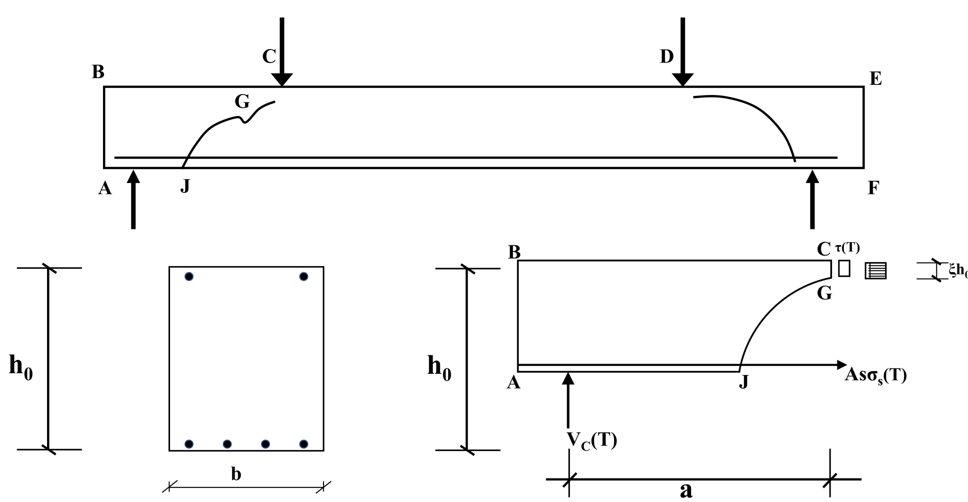

Figure 5: Calculation diagram for the thermo-mechanical behavior of an RC beam under fire exposure.

Under thermal-mechanical coupling, based on strength criteria and equilibrium conditions, it can be derived that:

$$\rho = \frac{A_s}{bh_0}, \xi = \rho \frac{\sigma_s(T)}{\sigma_c(T)} \tag{16}$$

$$\frac{\tau(T)}{f_c(T)} = 0.226 - 0.15\frac{\sigma_c(T)}{f_c(T)} \tag{17}$$

According to the above formula, the shear bearing capacity of the section is obtained:

$$V_c(T) = f_c(T)\, bh_0 \left(\frac{0.226 - 0.075\frac{\rho\sigma_s(T)}{f_c(T)}}{0.5 + 0.226\lambda\frac{f_c(T)}{\rho\sigma_s(T)}} \right) \tag{18}$$

The results indicate that at 600°C, concrete retains ~45%–50% of its ambient strength and steel yield strength decreases to ~48.7%, consistent with Tables 3 and 4. Comparison of theoretical predictions with FEM simulations shows discrepancies within 7%–10%, demonstrating that the implemented temperature-dependent material models accurately reproduce basic strength-of-materials behavior.

Table 3: Concrete compressive strength at elevated temperatures.

T (°C)	20	200	400	600	800
$f_c(T)$	40.2	35.8	29.4	17.9	6.2
$\frac{f_c(T)}{f_c}$ (20°C)	100%	89.5%	73.4%	44.8%	15.4%

Table 4: Steel reinforcement yield strength at elevated temperatures.

T (°C)	20	200	400	600	800
$f_y(T)$	360	360	360	175.2	38.4
$\frac{f_y(T)}{f_y}$ (20°C)	100%	100%	100%	48.7%	10.7%

3.2 Temperature Field Contour Map

During fire exposure, the temperature distribution across the beam cross-section exhibits a clear gradient that intensifies with increasing exposure time. As shown in Fig. 4, the simulated contours illustrate how heat progressively penetrates from the exposed surfaces inward. At 30 min (Fig. 6a), only a thin surface layer reaches elevated temperatures, while the beam core remains relatively cool. By 60–90 min (Fig. 6b,c), the high-temperature zone advances deeper into the section, and by 150 min (Fig. 6d), much of the cross-section is affected. The highest temperatures consistently occur at the bottom corners, near the longitudinal reinforcement, because these regions are exposed to two perpendicular fire surfaces, leading to localized heat accumulation, and accelerated temperature rise. Overall, the contours evolve into a characteristic "U-shaped" thermal profile, with cooler regions near the unexposed top face and hotter regions concentrated at the lower sides and bottom. This pattern reflects the combined effects of concrete's thermal inertia, which delays heat penetration, and the limited fire duration relative to the section's size.

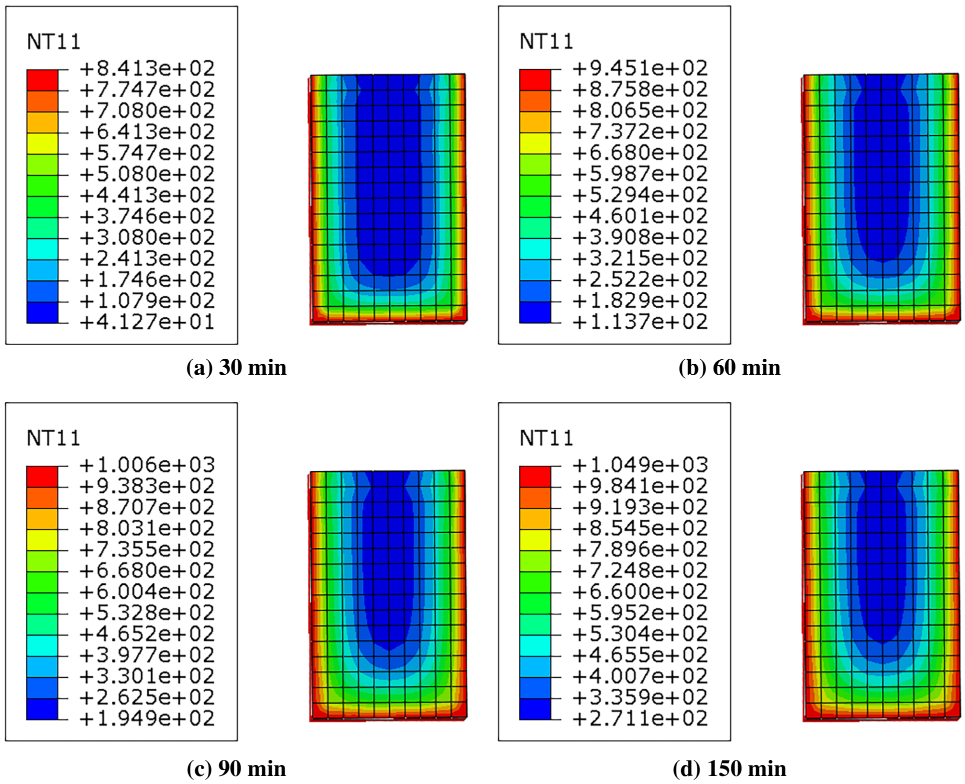

Figure 6: Temperature field (°C) in beam cross-section at mid-span: (**a**) 30 min fire exposure, (**b**) 60 min fire exposure, (**c**) 90 min fire exposure, (**d**) 150 min fire exposure.

3.3 Force Field and Crack Propagation Analysis

The mechanical response of the RC beams under fire exposure reflects the coupled effects of thermal expansion, material degradation, and structural constraints. As temperatures increase, significant thermal gradients develop across the beam depth, inducing tensile stresses in cooler regions and compressive stresses in the hotter concrete near the fire-exposed surfaces. These gradients promote progressive cracking and spalling of the cover concrete, particularly at the bottom corners where longitudinal reinforcement is located. By 500°C–600°C, the concrete's compressive capacity and the steel's tensile capacity are significantly reduced, causing stress redistribution toward the cooler interior [23]. The temperature-dependent degradation of bond strength amplifies differential deformation, as the SPRING2 elements representing the steel–concrete interface progressively lose stiffness, diminishing composite action and transferring tensile forces from steel to softened concrete.

The simulation captures the evolution of crack propagation and structural damage, showing that cracks initiate at the bottom corners and propagate upward through the web, eventually resulting in combined flexural and shear failure modes. By approximately 90–120 min into fire exposure, vertical and oblique cracks extend from the bottom corners upward, while the top portion of the section exhibits compressive crushing near mid-span. These numerical observations correspond closely to the experimental post-fire inspection, where visible cracks, spalling, and reinforcement exposure are observed prior to ultimate failure.

Fig. 7 illustrates the experimental post-fire behavior of the C40 RC beam, with (a) showing a simplified schematic of crack development and (b) presenting the actual post-fire failure pattern. Fig. 8 presents the simulated post-fire failure pattern, highlighting spalled cover, exposed reinforcement, and compression zone crushing. The close correspondence between Figs. 7 and 8 validates the predictive capability of the numerical model [24]. The progressive damage of the beam is illustrated in Fig. 9a–c by the distribution of maximum principal plastic deformation. At an early stage of the fire (30 min), plastic deformation is localized near the supports and exposed corners. As the fire continues (60 min), plastic strains gradually extend toward the mid-span. By 120 min, significant plastic deformation occurs across most of the beam section, particularly at the mid-span, indicating substantial weakening of structural integrity.

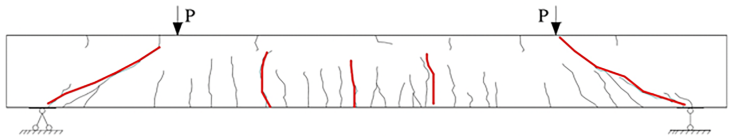

(a) Simplified diagram of cracks under applied load

(b) Experimental photograph showing visible cracks, spalling, and reinforcement yielding.

Figure 7: Post-fire crack propagation of the C40 reinforced concrete beam under ISO-834 fire exposure.

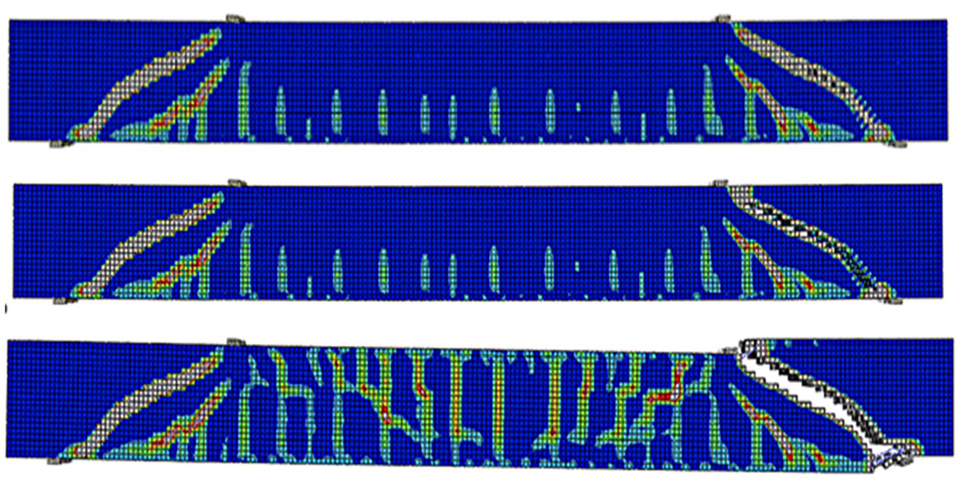

Figure 8: Simulated post-fire failure process and mode of an RC beam.

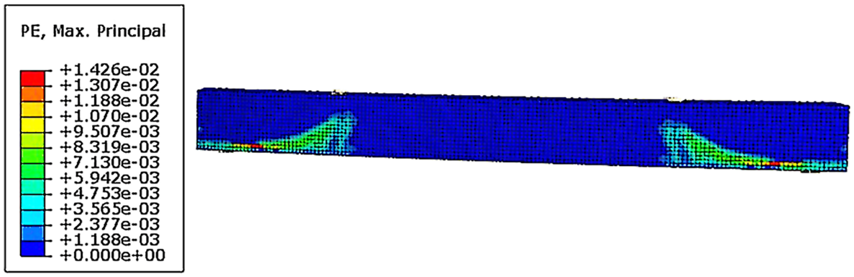

(a) 30 min

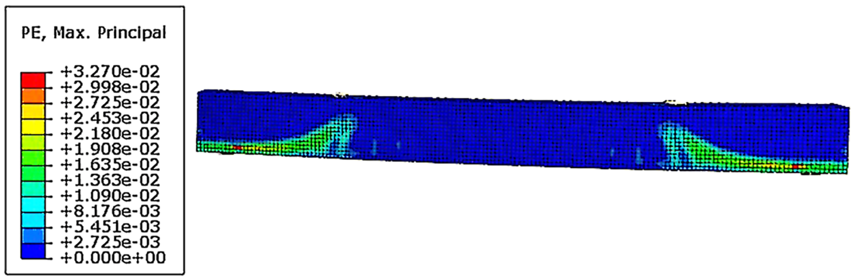

(b) 60 min

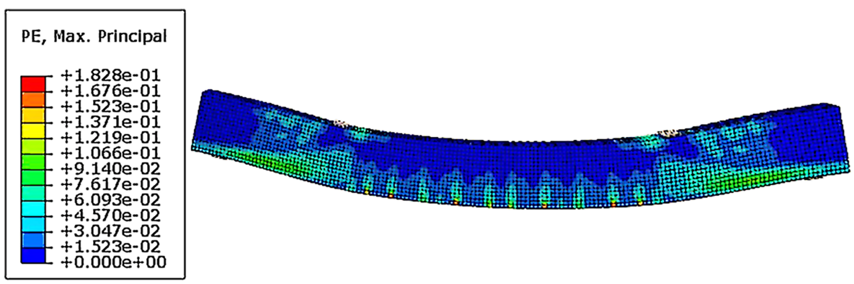

(c) 120 min

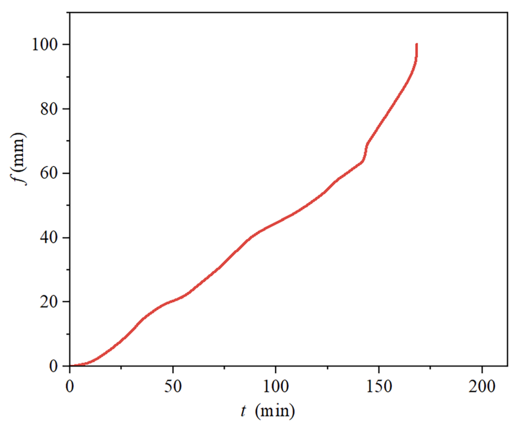

(d) Beam deflection curve obtained from Abaqus simulations

Figure 9: Evolution of deformation in RC beam under fire exposure.

Fig. 9d presents the corresponding beam deflection curve obtained from Abaqus simulations, which shows the progressive increase of mid-span deflection with fire duration. The deflection curve corresponds well with the regions of high plastic deformation, confirming that areas experiencing the largest stress and strain concentrations coincide with maximum beam deflection. This combined representation provides clear validation of the thermo-mechanical response of the beam under ISO-834 fire exposure.

3.4 Load–Midspan Deflection Relationship

The influence of progressive material degradation and bond-slip weakening on global beam behavior is illustrated through the load–midspan deflection curves (Fig. 10). Numerical simulations (red dashed lines) closely track experimental measurements (black solid lines) for all three beams. At ambient temperature, the initial stiffness is accurately reproduced, while progressive heating leads to reduced slope and peak load. For beam L1, the experimental ultimate load is approximately 80 kN with a 25 mm mid-span deflection, whereas the simulation predicts 85 kN at 22 mm. Beam L3 shows similar agreement, with experimental and numerical ultimate loads of 60 and 65 kN, respectively, and mid-span deflections of 30 vs. 28 mm. Minor deviations in later stages are attributed to simplified post-peak concrete behavior in the CDP model and approximations in bond-slip modeling. Overall, the numerical model effectively captures the progressive softening of the load–deflection response, reflecting reductions in stiffness, peak load, and residual capacity due to thermal and mechanical degradation.

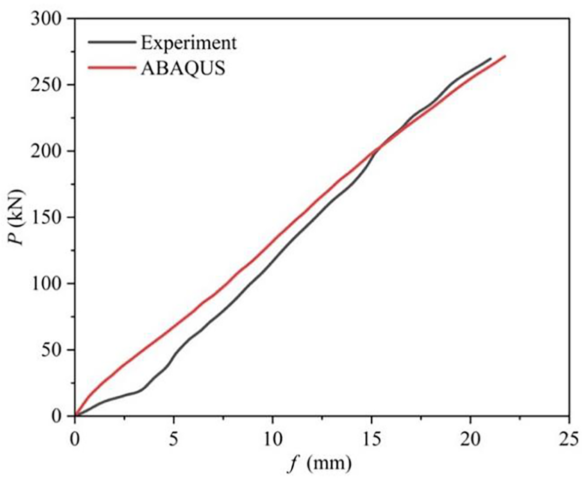

(a) L1 P–f curve

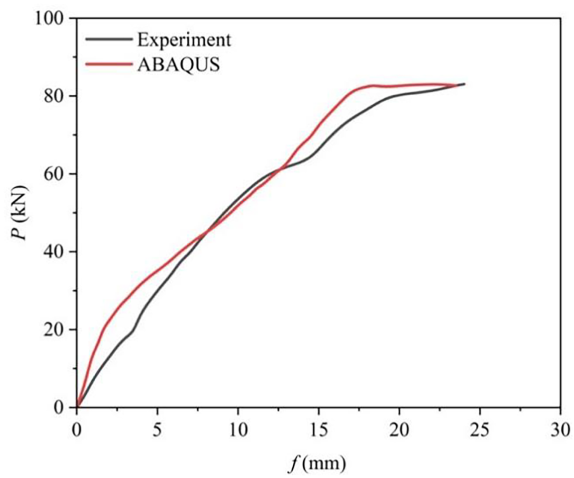

(b) L2 P–f curve

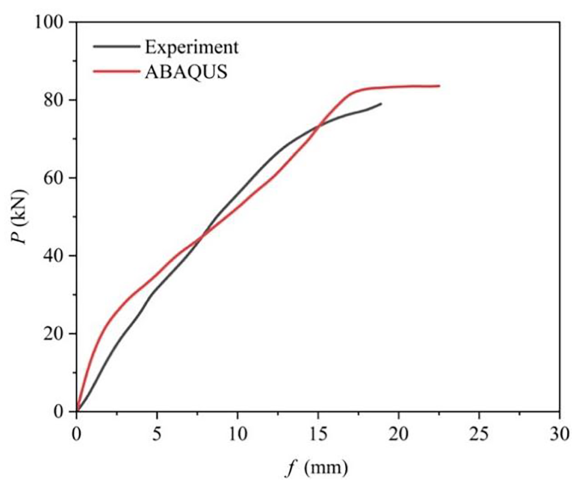

(c) L3 P–f curve

Figure 10: Load–mid-span deformation relationship (P–f curve) for RC beams under fire.

3.5 Residual Strength and Key Observations

The combination of thermal softening, steel yield degradation, and bond-slip deterioration collectively governs the residual load-bearing capacity of the beams after fire exposure. After two hours of fire exposure followed by natural cooling, the beams retain approximately 60%–70% of their load-carrying capacity at intermediate temperatures (~500°C–600°C) and drop to 20%–25% at extreme temperatures (~800°C) [25]. The simulation reproduces the experimental observations of extensive spalling, cover loss in tension zones, and compressive crushing in the upper regions of the cross-section. Fig. 9 shows the progressive development of plastic deformation over time, highlighting the spread from localized zones at early stages to widespread mid-span plasticity at 120 min. These results demonstrate that a sequentially coupled thermo-mechanical approach, integrating temperature-dependent concrete and steel constitutive laws and an explicit bond-slip formulation, can reliably predict both time-dependent deformation and residual load-bearing capacity [26]. The approach captures the interaction between thermal expansion, material softening, bond-slip, and crack propagation, providing a validated framework for post-fire performance assessment and supporting the design of fire-resilient reinforced concrete structures.

4 Conclusion

This study develops and validates a sequentially coupled thermo-mechanical numerical framework for reinforced concrete (RC) beams subjected to ISO-834 fire exposure. The model integrates temperature-dependent concrete damage plasticity, elastoplastic steel constitutive laws, and an explicit bond-slip mechanism, enabling the simulation of progressive degradation in concrete stiffness and strength, reduction of steel yield capacity, and deterioration of the steel–concrete interface. The framework captures the complex interaction between thermal gradients, material softening, and interface behavior, reflecting realistic beam responses during and after fire exposure.

Validation against load–midspan deflection curves demonstrates the accuracy of the proposed approach, with deviations within 7%–10% for all tested beams. Minor differences at high deflections are attributed to simplified post-peak concrete behavior and bond-slip modeling, yet the overall predictive capability remains robust. The results indicate that steep thermal gradients induce significant internal stresses and that the combination of concrete softening, steel yield reduction, and bond deterioration governs the evolution of internal forces and crack propagation. Explicit incorporation of bond-slip effects proved critical, as neglecting interface degradation would overestimate structural stiffness and residual load capacity, while the coupled model reproduces progressive deflections and failure modes observed experimentally.

The developed framework provides a practical and reliable tool for assessing post-fire structural performance, including mid-span deflection, internal stress distribution, crack evolution, and residual load-bearing capacity. It bridges experimental observations and numerical predictions, offering guidance for performance-based fire design of RC members.

Despite its effectiveness, certain limitations remain. The bond-slip model is simplified and may not fully capture interface degradation under extreme thermal gradients, while phenomena such as concrete spalling, moisture migration, and pore pressure effects were not explicitly modeled, which may lead to minor underestimation of mid-span deflections at later stages of fire. Moreover, the constitutive laws were based on Eurocode 2 and published models, which may not represent all variability in concrete mixes and steel grades, and the study focused on simply supported RC beams, without considering restrained or continuous members.

Future work will focus on refining bond-slip formulations, incorporating spalling and moisture mechanisms, and performing parametric and sensitivity analyses to quantify uncertainties. Extending the framework to other structural members, including slabs, columns, and composite systems, will enhance its applicability and support safer, more optimized performance-based fire engineering for reinforced concrete structures.

Acknowledgement: Not applicable.

Funding Statement: The authors received no specific funding for this study.

Author Contributions: The authors confirm contribution to the paper as follows: Conceptualization was done by Hongyan Liu and Feng Wu; methodology, software, formal analysis, data curation, writing of the original draft, visualization, and project administration were carried out by Hongyan Liu; validation was contributed by Hongyan Liu and Jie Zhao; investigation was performed by Fang Wang and Jie Zhao; writing—review and editing was handled by Hongyan Liu and Feng Wu; supervision was managed by Hongyan Liu. All authors reviewed and approved the final version of the manuscript.

Availability of Data and Materials: The data that support the findings of this study are available from the Corresponding Author, [Feng Wu], upon reasonable request.

Ethics Approval: Not applicable.

Conflicts of Interest: The authors declare no conflicts of interest.

References

1. Saha S, Serati M, Sahoo DR, Maluk C. Experimental and numerical analysis on the thermo-mechanical stresses triggering the onset of fire-induced concrete spalling. Fire Technol. 2025;61(5):3665–86. doi:10.1007/s10694-025-01749-3.
2. Hesien M, Youssef MA, El-Fitiany S. Finite element analysis of flat plate structures in fire. Fire. 2025;8(7):252. doi:10.3390/fire8070252.
3. Li Y, Liu F, Du T, Pan Y, Yang H, Li Y. Experimental behavior of axially loaded circular high-strength concrete-filled high-strength steel tubular stub columns after exposure to fire. Thin Walled Struct. 2024;203(2):112189. doi:10.1016/j.tws.2024.112189.
4. Zhang J, Chen J, Zhang R, Guo R. A numerical investigation of thermal-induced explosive spalling behavior of a concrete material using cohesive interface model. Front Phys. 2022;10:857381. doi:10.3389/fphy.2022.857381.
5. Feng W, Yang X, Raja Hussin TA. Thermodynamically consistent damage-plasticity model for fire-resistant design and optimization of reinforced concrete beams. Front Mater. 2026;12:1732117. doi:10.3389/fmats.2025.1732117.
6. Tang C, Bao Y, Yu Y. Study on the seismic performance of steel tube-reinforced concrete columns after fire on one side. Materials. 2025;18(9):1975. doi:10.3390/ma18091975.
7. Feng W, Hussin TAR, Yang X. A temperature-indexed concrete damage plasticity framework for thermomechanical analysis of concrete structures. J Eng Appl Sci. 2025;72(1):177. doi:10.1186/s44147-025-00753-2.
8. Ning J, Zhang L, Xu X. Virtual simulation for the dynamic response of concrete blocks under blast loading. Vis Comput. 2025;41(7):5171–87. doi:10.1007/s00371-024-03714-7.
9. Lu W, Ayoub A, D'Mello C. Effectiveness of coupled thermo-mechanical damage modelling in steel structural fire engineering. Fire Saf J. 2021;121(11):103314. doi:10.1016/j.firesaf.2021.103314.
10. Gernay T, Pei J, Tong Q, Bamonte P. Numerical analysis of the effects of fire with cooling phase on reinforced concrete members. Eng Struct. 2023;293:116618. doi:10.1016/j.engstruct.2023.116618.
11. Song Y, Fu C, Liang S, Li D, Dang L, Sun C, et al. Residual shear capacity of reinforced concrete beams after fire exposure. KSCE J Civ Eng. 2020;24(11):3330–41. doi:10.1007/s12205-020-1758-7.
12. Aliş B, Yazici C, Mehmet Özkal F. Investigation of fire effects on reinforced concrete members via finite element analysis. ACS Omega. 2022;7(30):26881–93. doi:10.1021/acsomega.2c03414.

13. Asghari Ghajari F, Yousefpour H. Residual bond-slip behavior in reinforced concrete members exposed to elevated temperatures. Struct Concr. 2023;24(3):3281–98. doi:10.1002/suco.202200927.
14. Gao WY, Dai JG, Teng JG, Chen GM. Finite element modeling of reinforced concrete beams exposed to fire. Eng Struct. 2013;52(4):488–501. doi:10.1016/j.engstruct.2013.03.017.
15. Rafi MM, Nadjai A. Behavior of hybrid (steel-CFRP) and CFRP bar-reinforced concrete beams in fire. J Compos Mater. 2011;45(15):1573–84. doi:10.1177/0021998310385022.
16. Rafi MM, Nadjai A. Numerical modelling of CFRP and hybrid reinforced concrete beams in fire. Fire Mater. 2013;37(5):374–90. doi:10.1002/fam.2135.
17. Tian J, Zhu P, Qu W. Study on fire resistance time of hybrid reinforced concrete beams. Struct Concr. 2019;20(6):1941–54. doi:10.1002/suco.201800320.
18. Neves IC, Rodrigues JPC, de Pádua Loureiro A. Mechanical properties of reinforcing and prestressing steels after heating. J Mater Civ Eng. 1996;8(4):189–94. doi:10.1061/(asce)0899-1561(1996)8:4(189).
19. Kodur VKR, Phan L. Critical factors governing the fire performance of high strength concrete systems. Fire Saf J. 2007;42(6–7):482–8. doi:10.1016/j.firesaf.2006.10.006.
20. Xu K, Zhang N, Yin ZY, Li K. Finite element-integrated neural network for inverse analysis of elastic and elastoplastic boundary value problems. Comput Meth Appl Mech Eng. 2025;436(3):117695. doi:10.1016/j.cma.2024.117695.
21. Wang Z, Wang J, Wu HN, Zhang R, Zhang GY, Zhang F, et al. Investigation of the microstructure, mechanical properties and thermal degradation kinetics of EPDM under thermo-stress conditions used for joint sealing of floating prefabricated concrete platform of offshore wind power. Constr Build Mater. 2025;485(5):141897. doi:10.1016/j.conbuildmat.2025.141897.
22. El-Hawary MM, Ragab AM, El-Azim AA, Elibiari S. Effect of fire on shear behaviour of R.C. beams. Comput Struct. 1997;65(2):281–7. doi:10.1016/S0045-7949(95)00356-8.
23. Wang Q, Yao B, Lu R. Behavior deterioration and microstructure change of polyvinyl alcohol fiber-reinforced cementitious composite (PVA-ECC) after exposure to elevated temperatures. Materials. 2020;13(23):5539. doi:10.3390/ma13235539.
24. Arioz O. Effects of elevated temperatures on properties of concrete. Fire Saf J. 2007;42(8):516–22. doi:10.1016/j.firesaf.2007.01.003.
25. Tao J, Yang XG, Lei Y, Wang C. Capturing rate- and temperature-dependent behavior of concrete using a thermodynamically consistent viscoplastic-damage model. Constr Build Mater. 2024;422:135791. doi:10.1016/j.conbuildmat.2024.135791.
26. Ergün A, Kürklü G, Başpınar MS. The effects of material properties on bond strength between reinforcing bar and concrete exposed to high temperature. Constr Build Mater. 2016;112(2):691–8. doi:10.1016/j.conbuildmat.2016.02.213.